HHS Public Access

Author manuscript

Nat Neurosci. Author manuscript; available in PMC 2010 August 01.

Published in final edited form as:

Nat Neurosci. 2010 February ; 13(2): 180–189. doi:10.1038/nn.2471.

HDAC1 nuclear export induced by pathological conditions is essential for the onset of axonal damage

Jin Young Kim[1], **Siming Shen**[1], **Karen Dietz**[2], **Ye He**[2], **Owain Howell**[3], **Richard Reynolds**[3], and **Patrizia Casaccia**[1,2]

[1] Graduate Program in Neuroscience at the Graduate School of Biomedical Sciences, University of Medicine and Dentistry of New Jersey-Robert Wood Johnson Medical School, 675 Hoes Lane, Piscataway, NJ 08854

[2] Department of Neuroscience and Genetics & Genomics, Mount Sinai School of Medicine. One Gustave Levy Place. Box 1065. New York NY 10029

[3] Department of Cellular and Molecular Neuroscience, Division of Neuroscience and Mental Health Imperial College Faculty of Medicine, Charing Cross Hospital Campus, London, UK

Abstract

Histone deacetylase 1 (HDAC1) is a nuclear enzyme involved in transcriptional repression. We report here that cytosolic HDAC1 is detected in damaged axons in brains of human patients with Multiple Sclerosis and of mice with cuprizone-induced demyelination, *ex vivo* models of demyelination and in cultured neurons exposed to glutamate and TNF-α. Nuclear export of HDAC1 is mediated by the interaction with the nuclear receptor CRM-1 and leads to impaired mitochondrial transport. The formation of complexes between exported HDAC1 and members of the kinesin family of motor proteins hinders the interaction with cargo molecules thereby inhibiting mitochondrial movement and inducing localized beadings. This effect is prevented by inhibiting HDAC1 nuclear export with leptomycin B, treating neurons with pharmacological inhibitors of HDAC activity or silencing HDAC1 but not other HDAC isoforms. Together these data identify nuclear export of HDAC1 as a critical event for impaired mitochondrial transport in damaged neurons.

INTRODUCTION

Axonal damage has been described in several neurodegenerative disorders[1] and in inflammatory demyelination, such as multiple sclerosis (MS)[2]–[4]. The morphological changes associated with axonal damage include the presence of localized axonal swellings,

Correspondence should be addressed to Patrizia Casaccia: patrizia.casaccia@mssm.edu.

Author Contribution

The majority of the experiments in the manuscript were conducted by Jin Young Kim. Siming Shen performed the first experiments in the demyelinated mice and the first mass-spectrometry data. Karen Dietz performed the in vivo confocal analysis in demyelinated mouse brains and the SAPK experiments, Owain Howell and Richard Reynolds performed the analysis of the human material, Ye He performed the qt-PCR experiments. Patrizia Casaccia designed the experimental plan, supervised the project and wrote the manuscript,

characterized by the succession of enlargements and constrictions along the axon (i.e. “beads-on-a-string” appearance) and the detection of “ovoids” or “end bulbs”, resembling the terminal stumps of transected axons[3,4]. Axonal transections have been considered a hallmark of irreversible axonal degeneration[3,5], and the presence of ovoids in the proximal part of the axons is typically associated with rapid retrograde degeneration[6] and neuronal death[7,8]. These neuropathological findings can be detected in distinct neurodegenerative disorders and thereby suggest that they might share a similar mechanism of induction of axonal damage.

A marker of axonal damage is the immunoreactivity with antibodies for the hypophosphorylated form of neurofilament heavy chain (SMI32). Neurofilaments, the unique axonal cytoskeletal molecules consist of three subunits classified on the basis of molecular weight: 200kDa heavy (NFH), 150kDa medium (NFM) and 68kDa light (NFL) chains. In physiological conditions, these subunits are phosphorylated and the degree of phosphorylation correlates with axonal caliber and speed of axonal transport[9], possibly by affecting the association of neurofilaments with the motor protein kinesin[10]. Hypophosphorylated neurofilaments in contrast, are characterized by enhanced susceptibility to protease digestion[11], greater tendency to self-aggregate[12], co-localization with tumor necrosis factor-α (TNF-α) immunoreactivity[13] and they are typically detected on the brain of animal models of demyelination[14] and MS patients[15].

Although the molecular mechanism linking axonal transport and neuropathology is not well characterized, many studies have reported that disruption of axonal transport[16] results in the rapid accumulation of proteins at the sites of swelling[17]. High concentrations of glutamate in cultured neurons have been shown to impair neurofilament transport and induce cytoskeletal protein accumulation at the sites of axonal swelling[18], thereby suggesting a causal relationship between localized swellings and local disruption of axonal transport[19]. Impaired axonal transport is likely to eventually trigger Wallerian degeneration of distal axons, and therefore it can be considered one of the first signs of damage which is associated with localized swelling and ultimately leads to transection.

Several pathological stimuli can negatively affect axonal transport, including accumulation of mutant proteins, cytoskeletal disorganization, excitotoxicity and altered histone deacetylase (HDAC) activity[17,20]. HDACs are a family of enzymes originally named after their ability to remove acetyl groups from lysine residues located within the N-terminal tail of histones, causing compaction of chromatin and repression of transcription[21,22]. On the basis of their primary structure, HDACs can be further classified as class I (HDAC1, 2, 3, and 8), Class II (HDAC 4, 5, 6, 7 and 9) and Class III (SIRT1–7)[21],. It has now been defined that HDACs also modulate the activity of non-histone proteins such as YY1[23] and NF-kB[24]. In addition, class II HDACs are cytosolic enzymes removing acetyl groups from the epsilon position of lysine residues of cytosolic proteins, including α-tubulin[25]. Class II HDACs, HDAC4 and HDAC5 shuttle in and out of the nucleus. In physiological conditions, they are detected in the cytoplasm[21]. In pathological conditions, (i.e. Huntington’s disease), however HDAC5 is detected in the nucleus where it is thought to repress gene expression[26]. Acetylation of α-tubulin regulated by a microtubule-associated deacetylase, HDAC6[25], has been shown to negatively affect axonal transport by removing acetyl groups from α-tubulin,

thereby impairing its ability to recruit the motor proteins kinesin-1 and dynein to microtubules. In agreement with the negative effect of HDAC6 in vesicular transport, it has been noted that this molecule is a component of Lewy bodies in Parkinson's disease[27], while in Huntington's disease it has been associated with defective release of neurotrophic factors[28]. These studies have suggested that axonal transport is negatively regulated by HDAC6-dependent deacetylation of α-tubulin in neurodegenerative disorders.

Impaired axonal transport has also been correlated with cytoskeletal disorganization caused by the proteolytic degradation of cytoskeletal proteins induced by calcium activated proteases[29]. It has been proposed that excess Ca^{2+} activates Ca^{2+}-dependent proteases such as calpain and caspases which act on several substrates, most of which are cytoskeletal proteins[29]. However it is unclear whether calcium entry and HDAC activity are independent mechanisms associated with early and late stages of axonal damage.

This study describes the neuronal specific and calcium-dependent nuclear export of HDAC1 in demyelinating conditions and in neurons exposed to excitotoxic amino acids and cytokines, in order to mimic the inflammatory environment characteristic of the demyelinated brain[30]. We identify molecular events responsible for morphological changes of neurites that are independent of HDAC6-mediated tubulin deacetylation and dependent on a cytotoxic function of cytosolic HDAC1.

RESULTS

HDAC1 nuclear export in damaged axons

Previous studies reported that the axonal changes detected in the brain of MS patients can also be observed in the corpus callosum of mice with cuprizone-induced demyelination [14,31]. Therefore, we processed brain sections from C57BL/6J mice maintained on a 0.2% cuprizone diet for 4 (n = 9) or 6 weeks (n = 6) or on a regular diet (n = 15). To test the hypothesis that histone deacetylases could be involved in axonal damage induced by neuroinflammation, we focused our analysis on callosal axons in the 4week group, because at this time point we can detect demyelination associated with extensive microglial infiltration and axonal damage [31,32]. We used antibodies specific for class I and class II HDACs and for neurofilament medium chain to identify callosal axons. No difference in the subcellular localization of class I and II HDAC isoforms was detected in cuprizone-treated and control mice (Fig. 1a), with the exception of HDAC1, that showed a more prominent cytosolic localization in the corpus callosum of cuprizone-treated animals, especially in areas associated with microglial infiltration (Fig. 1a) and axonal damage (Fig. 1b). The protein levels for the distinct HDAC isoforms remained unchanged throughout the duration of the cuprizone treatment (Supplementary Fig. 1, n = 3 mice per time point). Cytoplasmic HDAC1 was also detected in sections from brain blocks that were selected from four cases of neuropathologically confirmed MS. Tissues were sampled from the superior frontal gyrus by selecting those containing macroscopically visible lesions. The areas of interest were screened for the presence of demyelination, using Luxol fast blue/periodic acid Schiff staining (Fig. 1c). The immunoreactivity of SMI32, an antibody specific for the hypophosphorylated form of neurofilaments heavy chain, was evaluated in twenty nine areas of interest within the demyelinated regions. The number of $HDAC1^+$ and $SMI32^+/HDAC1^+$

profiles was quantified per 400× microscopic field (0.29mm^2). No HDAC1$^+$/SMI32$^-$ profiles were noted. The average number of HDAC1$^+$ processes expressed per mm^2 was 7.55±1.8 (mean ± SE) while the average number of SMI32$^+$ neurites was 29.8±6.1 (mean ± SE). Thus co-localization was detected in 25.3% of damaged axons, identified by immunoreactivity for SMI32 (Fig. 1d–e).

HDAC1 translocation was also detected in an *ex vivo* model of inflammatory demyelination, induced by exposure of cerebellar slice cultures to lysolecithin and lipopolysaccharide (LPS) to induce demyelination[33] and microglial activation. Using immunohistochemistry with antibodies specific for NFM-L and for myelin basic protein (MBP) to identify demyelination, we detected multiple beaded axons in demyelinated white matter regions in the presence of activated microglia (Fig. 1f). These axons were also immunoreactive for HDAC1 and SMI32 (Fig. 1g), thereby confirming the cytoplasmic localization of HDAC1 at the early stages of axonal damage following demyelination and microglial activation.

HDAC1 nuclear export precedes the onset of axonal damage

It has been previously proposed that glutamate and cytokines produced by microglial cells can be neurotoxic and therefore we exposed primary neuronal cultures to glutamate and cytokines in order to best mimic the inflammatory environment in the brain of MS patients[30]. Immunocytochemistry was used to characterize the cellular composition of the neuronal cultures (Supplementary Fig 2 a–b), and increasing concentrations of glutamate together with a constant amount of cytokines (i.e.200ng/ml of TNF-α), were tested for the ability to induce neurite pathology. The lowest concentration (50μM glutamate and 200ng/ml TNF-α) that induced neuritic beading within 2 hours of exposure was chosen to perform a time-course experiment of axonal damage, using immunoreactivity for SMI32 and morphological appearance of beaded neurites as detection criteria. In agreement with the progressive nature of damage, after 2 hours 42.88±8.06% of the neurites displayed the characteristic beaded morphology and 20.6±9.46 % were also SMI32$^+$; after 24 hours 88.07±1.98 % displayed beadings and 61.58±2.23% were SMI32$^+$ (Fig. 2a–b). To confirm the relationship between localized beadings and later signs of damage we conducted live-imaging on neurons before and after treatment with glutamate and TNF-α and followed the morphological changes occurring during the following 12 hours, using time-lapse video microscopy. During the first 2 hours we detected a progressive increase in the percentage of beaded neurites, that was later replaced by the detection of transections, a hallmark of late stages of axonal damage (Fig. 2c–d), and that was associated with decreased neuronal viability (Supplementary Fig. 3).

The progressive nature of the morphological changes detected in the neurites after treatment with glutamate and TNF-α, correlated with the progressive changes of HDAC1 subcellular localization. Prior to exposure to excitotoxic amino acids and cytokines, HDAC1 was detected within the nuclear compartment (Fig. 3a). However, within the first five minutes of treatment it was observed in a perinuclear location (Fig. 3a), by twenty minutes HDAC1 was evenly distributed along the entire length of the neurites and at 2 hours, it formed aggregates within the enlargements of the beaded neurites (Fig. 3a–b). Based on these results we hypothesized that nuclear export of HDAC1 was part of the mechanism leading to neuronal

damage. Previous evidence had suggested that localized enlargements and beading were associated with disrupted axonal transport with consequent accumulation of proteins and organelles[16]. Labeling of treated primary cultured neurons with the cell-permeable mitochondrial dye MitoTracker Green FM (Invitrogen) followed by time-lapse video microscopy, allowed the visualization of all the moving mitochondria (Fig. 3c). The average speed of mitochondrial transport in untreated primary neurons was 0.23±0.04 μm s^{-1}. After 5 minutes of treatment, when HDAC1 was detected in perisomatic locations but not yet in the neurites, mitochondrial transport was still 0.21±0.07 μm s^{-1}. At 20 minutes, however, when HDAC1 reached the neurites, mitochondrial transport was significantly decreased (x=0.089±0.012 μm s^{-1}). By two hours, the average speed was decreased even more (x=0.038±0.029 μm s^{-1}) and this correlated with the detection of localized neurite swellings (Fig. 3d). Thus, impaired mitochondrial transport preceded the appearance of localized beadings.

To address the possibility that the subcellular localization of other HDAC isoforms was similarly affected, we repeated immunocytochemistry in primary neurons, cultured for two hours in the presence of glutamate and TNF-α, using antibodies specific for each isoform and DAPI as nuclear counterstain (Supplementary Fig. 4). Of all the HDAC members analyzed, HDAC3, HDAC4, HDAC6 and HDAC8 were also detected in the cytoplasm. However, HDAC1 was the only isoform that was exported from the nucleus and accumulated in the neurites in response to glutamate and TNF-α treatment (Supplementary Fig. 4). To further confirm the nuclear export of HDAC1, we repeated the experiment using three distinct HDAC1 antibodies, including two commercially available ones generated against the C-terminus and one against the N-terminus of the molecule (Supplementary Fig. 5). The same results were detected with all three reagents. Inducible HDAC1 nuclear export was cell-type specific, since it was detected in primary neurons, but not in astrocytes or oligodendrocytes receiving the same treatment (Supplementary Fig. 6). To further validate the inducible nuclear export of HDAC1 using an alternative approach we expressed a FLAG-tagged HDAC1 molecule in neurons, and tracked its subcellular localization in response to glutamate and TNF-α treatment, using an anti-FLAG antibody (Fig. 4a). While in the absence of any treatment, over-expressed FLAG-tagged HDAC1 was detected exclusively in the nuclei of transfected neurons, after treatment with glutamate and TNF-α, the FLAG-tagged HDAC1 was first detected in perinuclear locations and then distributed all along the neurites (Fig. 4b).

Because axonal damage in demyelinating disorders is not limited to areas of acute demyelination[34], it has been proposed that damage could be caused by calcium entry in response to distinct causes, including myelin loss[5], activation of glutamate receptors[35] or cytokine-mediated release from intracellular stores[36]. To determine whether HDAC1 nuclear export was downstream of calcium entry, we pre-treated neurons with increasing concentrations of the calcium chelator EDTA for 30 minutes prior to exposure to 50μM glutamate and 200ng/ml TNF-α for 2 hours. Cultures were then processed for immunocytochemistry using specific antibodies against HDAC1 and neurofilaments. EDTA pre-treatment prevented the onset of neurite beading in a dose-dependent manner, with a maximum effect at a concentration of 10mM (Fig. 4c), which correlated with retention of

HDAC1 in the nucleus. Thus, HDAC1 nuclear export in response to glutamate and TNF-α treatment required the presence of calcium.

Silencing of HDAC1 prevents neuritic beading

To further define the role of HDAC1 in the induction of neuritic beading, we adopted a silencing approach and tested a minimum of four lentiviral targeting constructs for each HDAC isoform, for efficiency and specificity of silencing and selected the two most promising ones (Supplementary Fig. 7). Primary neurons were transduced with these shRNAs and 72 hours later, they were treated with glutamate and TNF-α. Mock infected cultures were used as controls (Fig. 5a). Silencing of *Hdac1* prevented the appearance of beaded neurites. While the percentage of beaded neurites in mock infected neurons was 58.1±1.65% (n = 35±2.8), the silencing of *Hdac1* with shRNA decreased the percentage of beaded neurites to 19.4±2.4% (n = 34±2.1). Silencing of other members of class I (i.e. *Hdac2*, *Hdac3* and *Hdac8*) and class II (i.e. *Hdac4* and *Hdac6*) histone deacetylases, in contrast, did not elicit the same effect (Fig. 5b). Together these results support a critical role for HDAC1 in the onset of neurite beading.

CRM1-dependent HDAC1 export is essential for axonal damage

Since HDAC1 is a nuclear enzyme, we reasoned that it must be exported from the nucleus by a process that is initiated by exposure to pathological stimuli. For class II HDACs, shuttling from the nucleus to the cytoplasm has been attributed to the presence of Nuclear Export Signals (NESs)[21], that allows binding to the Exportin 1 receptor (CRM1), followed by transport through the nuclear pore. The original consensus sequence for nuclear export and CRM1 binding was identified as LXXXLXXLXL[37]. Amino acid sequence analysis of HDAC1 using the ScanProsite program (Expert Protein Analysis System, Switzerland) revealed the presence of leucine-rich residues (LXXXLXXL or LXXLXL, Fig. 6a), similar to the NES that was originally described in viral proteins[37]. Therefore we hypothesized that nuclear export of HDAC1 could be mediated by the interaction of specific leucine residues within the putative NES, with CRM1. Protein extracts from neuronal cultures exposed to glutamate and TNF-α for 5 and 20 minutes, were immunoprecipitated with HDAC1 antibodies followed by western blot analysis. A complex between CRM1 and HDAC1 (Fig. 6b) was detected during the first 5 minutes of treatment, but not at later time points (Fig. 6b). To further confirm that this interaction was mediated by the NES sequence on HDAC1, we generated a C-terminal FLAG-tagged point mutant, by converting leucine→alanine residues within the putative NES. Overexpression of this mutant HDAC1, interfered with the formation of a complex with CRM1 (Fig. 6c), thereby supporting a functional interaction between the putative NES sequence in HDAC1 and CRM1.

The functional significance of HDAC1 nuclear export was then tested with leptomycin B (LMB), a pharmacological inhibitor of CRM1-dependent transport[38]. Pre-treatment of neurons with increasing concentrations of LMB for 30 minutes prior to exposure to glutamate and TNF-α, prevented HDAC1 export from the nucleus and inhibited neurite beading in a dose-dependent manner (Fig. 6d–e). Pre-treatment of cultured neurons with doses of LMB that prevented HDAC1 nuclear export also had important effects on mitochondrial transport. While 84% decreased in the speed of mitochondrial transport was

detected in cultures exposed to glutamate and TNF-α compared to untreated controls, LMB pre-treatment significantly ameliorated the ability of mitochondria to move even in the presence of glutamate and TNF-α, although it was unable to restore the speed to that measured in controls (Fig. 6f–g). Together these results suggest that CRM1-mediated nuclear export of HDAC1 is part of the mechanism that modulates mitochondrial transport in pathological conditions associated with localized neurite swellings and beading.

Cytosolic binding partners for HDAC1 in damaged axons

Since HDAC1 nuclear export decreased its bioavailability in the nucleus, it was conceivable that impaired mitochondrial transport could be consequent to decreased nuclear function, rather than acquisition of a cytosolic function. Histone H3 is one of the major nuclear substrates for HDAC1, therefore we assessed the effect of glutamate and TNF-α treatment on the levels of acetyl-H3 (Supplementary Fig. 8a) and on the transcript levels of genes previously shown to be regulated by HDAC1[39–42]. Increased levels of acetyl-H3 were not detected until two hours and no change in the levels of transcripts involved in apoptosis (i.e. *Bax* and *c-Jun*), survival (i.e. *Bcl2*) or axonal damage (i.e. *Nav1.2*, *Nav1.6* and *c-Jun*) was detected (Supplementary Fig. 8b). Because the first localized signs of beadings were observed as early as 20 minutes after exposure to glutamate and TNF-α, well before any change in acetyl-H3 could be measured, we concluded that the effect of HDAC1 nuclear export on neuritic damage was likely due to a cytosolic gain of function rather than loss of its nuclear function.

To mechanistically define the role of cytosolic HDAC1 in axonal damage and find potential binding partners in the axons of damaged neurons, we adopted an unbiased approach, and performed MALDI-TOF Mass Spectrometry on protein extracts isolated from callosal axons of control and cuprizone-treated mice and from untreated or glutamate and TNF-α treated neuronal primary cultures, immunoprecipitated with anti-HDAC1 antibodies. The experiment was independently repeated on three distinct animal groups and three groups of neuronal cultures. Only molecules that were identified as binding partners in all the 6 independent samples (3 *in vivo* experiments and 3 *in vitro* experiments) were further processed for validation analysis, using immunoprecipitation and western blot of protein extracts from the corpus callosum of untreated mice ($n = 7$) and of mice treated with cuprizone for 4 ($n = 7$) or 5 weeks ($n = 4$). The results obtained after immunoprecipitation with anti-HDAC1 antibodies were compared with those obtained with anti-HDAC4 and anti-HDAC6 antibodies (Fig. 7a). In agreement with previous reports[43] α-tubulin was a prominent band immunoprecipitated by HDAC6 antibodies in extracts from both control and treated groups (Fig. 7a). Tubulin was not precipitated by anti-HDAC4 antibodies while the interaction of HDAC1 with cytoskeletal elements (i.e. α-tubulin) and with proteins involved in axonal transport (i.e. KIF2A) was detected only in cuprizone-treated mice (Fig. 7a). These data identified differential binding for distinct histone deacetylases to proteins involved in mitochondrial transport (Fig. 7a). The inducible interaction between HDAC1 and proteins involved in axonal transport was detected only in brain regions characterized by microglial infiltration and cytokine production (i.e. corpus callosum), but was not detected in non-demyelinated areas (i.e. spinal cord) (Fig. 7b).

Previous studies related impaired axonal transport in models of Huntington's disease to deacetylation of α-tubulin mediated by HDAC6, and suggested a positive effect of treatment with HDAC6 inhibitors on axonal transport[28]. In our experimental system, however, the impaired mitochondrial transport was not ameliorated by the presence of pharmacological inhibitors of HDAC6 (i.e. tubacin, Fig. 8a–b), that increased the acetylation of α-tubulin. These results well correlated with the observation of similar levels of acetyl-tubulin in control and cuprizone treated mice (Supplementary Fig 9a–b) and in neurons untreated or treated with glutamate and TNF-α (Supplementary Fig. 9c). Together, these results support the concept that distinct HDAC isoforms are differentially involved in the induction of axonal damage caused by different stimuli.

The detection of cytosolic HDAC1, rather than HDAC6 in response to neuronal exposure to glutamate and cytokines, suggested a possible role of HDAC1 inhibitors in the improvement of mitochondrial transport. Indeed, mitochondrial transport in glutamate and TNF-α treated neurons was significantly better in the presence of the HDAC1 inhibitor MS-275 (Fig. 8a–b) than in its absence or in the presence of the HDAC6 inhibitor tubacin (Fig. 8a–b), thereby supporting an HDAC1-dependent mechanism of impaired mitochondrial transport. The effectiveness of MS-275 and tubacin in modulating mitochondrial transport in neurons treated with glutamate and TNF-α correlated with the protective role of MS-275, but not tubacin in the induction of neurite beading (Fig. 8c–d). Thus, while HDAC1 inhibitors improved mitochondrial transport and prevented damage, HDAC6 inhibitors did not protect from damage induced by exposure to both glutamate and TNF-α.

Because the acetylation status of α-tubulin was not affected by our experimental paradigm, we reasoned that HDAC1 modulation of axonal transport must include the involvement of other binding partners. The most likely candidates were the motor proteins KIF2A and KIF5, as identified by MALDI-TOF. Therefore, we conducted immunoprecipitation of extracts from neurons either untreated, or treated with glutamate and TNF-α with antibodies for HDAC1 or HDAC6 and assessed the identity of the binding partners by western blot analysis, using antibodies specific for α-tubulin, KIF2A, KIF5 and for the cargo molecule dynamin (Fig. 8e). As predicted by the *in vivo* results, the interaction between α-tubulin and HDAC1 was detected only after 20 minutes of treatment and was coincident with the first detection of impaired mitochondrial transport, while the interaction with HDAC6 was constitutive (Fig. 8e). Interestingly, there was a switch in the ability of KIF2A to bind distinct isoforms. While in untreated neurons KIF2A was predominantly bound to HDAC6, in treated neurons this interaction was detected primarily with HDAC1 (Fig. 8e). Finally, while HDAC6 was able to bind dynamin, no interaction was detected between this molecule and HDAC1. These interactions required the specific activity of distinct HDAC isoforms, since only treatment with MS-275 but not with tubacin, prevented the interaction of HDAC1 with the motor proteins (Fig. 8e). Since HDAC1 interacted with motor proteins, but not with dynamin, we asked whether the ability of this protein to bind with KIF2A and KIF5 was inversely correlated with HDAC1 binding. Indeed, in untreated neurons, dynamin was found in complex with KIF2A, KIF5 and α-tubulin (Fig. 8f). Exposure to glutamate and TNF-α disrupted this interaction despite the constant protein levels of these molecules (Fig. 8g). Co-treatment with the HDAC1 inhibitor MS-275, in contrast, partially rescued complex

formation between KIF2A, KIF5, α-tubulin and dynamin (Fig. 8f). HDAC1 silencing also restored binding of dynamin with α-tubulin, but only partially restored the interaction with motor proteins (Fig. 8f). The lack of complete reversion of the effect could be explained by taking into account the efficiency of silencing in primary neurons (Supplementary Fig. 7a) or by implying the existence of additional mechanisms modulating the glutamate-dependent effect on axonal transport. Based on these results we conclude that neuroinflammatory stimuli, including excitatory amino acids and cytokines, induce calcium-dependent HDAC1 nuclear export. Cytosolic HDAC1 binds to α-tubulin and kinesin motors (i.e. KIF2A and KIF5) in an activity-dependent fashion, thereby disrupting the formation of functional interactions between these motor proteins and dynamin on cargo (Supplemental Fig. 10). The impaired axonal transport, coincident with the areas of aggregation of HDAC1/motor protein complexes might contribute to localized areas of swelling that eventually lead to irreversible transections. Therefore, the definition of the molecular interactions between motor proteins, dynamin, α-tubulin and HDAC1 will likely provide a better understanding on how to restore mitochondrial transport and axonal function.

Discussion

Axonal damage detected in inflammatory demyelination, such as multiple sclerosis[2,3], has been associated with impaired mitochondrial function[5] and related to calcium entry, due to aberrant activation of sodium channels or activation by excitatory amino acids and cytokine production[17,20]. However the molecular mechanisms linking defective mitochondrial function to calcium entry remained elusive. In this study we identify calcium-mediated nuclear export of HDAC1 as a critical modulator of impaired mitochondrial transport and the induction of axonal damage in inflammatory demyelination. Cytosolic HDAC1 was detected in the brains of patients with multiple sclerosis, in animal models of demyelination characterized by microglial infiltration and cytokine production[14,31], and in cultured neurons exposed to excitatory amino acids and cytokines to mimic the inflammatory environment of the MS brain[30]. Previous studies in other neurodegenerative disorders have focused on the neurotoxic effect of nuclear localization of other isoforms of cytosolic HDACs and suggested that neurotoxicity was the result of HDAC-dependent repression of survival genes[44,45]. Our results, in contrast, suggest a cytotoxic role for the exported HDAC1 that is independent of its nuclear function and that is part of the mechanism impairing mitochondrial transport and inducing neurite beading in response to excitatory amino acids and cytokines. The neuroprotective effect of leptomycin B treatment, a pharmacological blocker of CRM1-mediated nuclear export, suggested that the role of HDAC1 in axonal damage required a cytosolic, rather than nuclear localization. If nuclear export of HDAC1 impaired mitochondrial transport due to its effect on the transcription of pro-apoptotic genes, then acetylation of nuclear substrates and changes in gene expression should have kinetics that precede impaired mitochondrial transport. Acetylation of nuclear histones and altered gene expression, in contrast, were detected only at later stages. Thus, we conclude that axonal damage is mediated by a gain of cytosolic function for HDAC1 rather than loss of a protective nuclear function. The toxic effect of cytosolic HDAC1 on axonal transport is consequent to its ability to bind to motor proteins (i.e. KIF2A and KIF5) and α-tubulin, disrupting their ability to form complexes with cargo proteins (i.e. dynamin).

These complexes were detected in demyelinated brain regions in animal models characterized by cytokine production by microglial cells (i.e. corpus callosum) and in neurons exposed to glutamate and cytokines, but not in non-demyelinated regions (i.e. spinal cord) or in untreated cultures.

A role for cytoplasmic HDAC6 in the inhibition of axonal transport had been previously suggested for pathologies characterized by intracellular accumulation of misfolded proteins[28]. This role was attributed to the ability of HDAC6 to deacetylate α-tubulin[25]. Since α-tubulin deacetylation decreases its ability to recruit motor proteins, it was suggested that HDAC6-mediated inhibition of axonal transport decreased the vesicular transport of neurotrophic factors, and negatively affected neuronal survival[28]. Our results however, in a model of axonal damage associated with inflammatory demyelination suggest a mechanism of impaired axonal transport that is independent of HDAC6. Deacetylation of α-tubulin was not significantly changed in cultured neurons exposed to glutamate and cytokines or in animal models of demyelination. In addition, only silencing of HDAC1 and treatment with pharmacological inhibitors of HDAC1 activity (i.e. MS-275) but not of HDAC6 activity (i.e. tubacin), were able to improve mitochondrial transport, prevent the disruption of complexes between cargos and motor proteins and reduce the formation of axonal swellings. It is important to mention that the improvement detected in the presence of pharmacological inhibitors or in response to HDAC1 silencing, was not a complete reversion of the toxic effect of glutamate and TNF-α treatment. Previous studies have discussed the importance of phosphorylation of motor proteins in disrupting axonal transport[46]. We cannot formally exclude the possibility that some of these mechanisms of impaired axonal transport, might still occur in the presence of HDAC inhibitors or HDAC1 silencing and be partially responsible for the incomplete rescue.

We suggest that distinct neurological disorders might share the morphological appearance of damage (i.e. beaded neurites), by differential involvement of distinct HDAC isoforms. In the case of Huntington's disease, impaired transport consequent to α-tubulin deacetylation is mediated by HDAC6, while in neuroinflammation impaired transport is caused, at least in part, by HDAC1 nuclear export and sequestration of motor proteins into protein complexes that alter mitochondrial transport.

The concept of cytoplasmic retention of HDAC1 in pathways associated with inflammation is supported by studies in other cellular systems. Even though a vast literature focuses on the nuclear role of HDAC1, a few studies in neuroblastoma cells[47],[48] reported the translocation of HDAC1 to the cytoplasm in response to HSV-1 viral infection. In addition, in 293 and Hela cells, the NFκB inhibitor IκBα was shown to interact with HDAC1 and HDAC3 and sequester these proteins in the cytoplasm[49]. We therefore conclude that distinct HDAC isoforms have the ability to negatively regulate axonal transport by interrupting the motor protein-microtubule interaction in a context-specific fashion that is dependent on the cell type and on the pathological stimulus. HDAC6, for instance, plays a critical role for axonal pathology associated with misfolded proteins, while HDAC1 plays an important role in axonal damage associated with neuroinflammation. The identification of HDAC1 nuclear export as event downstream of calcium entry in response to excitatory amino acids and cytokines treatment defines an important molecular target for pathologies associated with

inflammation. Future studies on the molecular characterization of the events leading to altered axonal transport might lead to the identification of novel therapeutic targets preventing the irreversibility of axonal transections.

Methods

Antibodies for immunohistochemistry (IHC), immunocytochemistry (ICC) and western blot (WB)

We used the following antibodies: neurofilament medium chain antibodies (Upstate; Chemicon), 1:300 for IHC and ICC; anti-neurofilament light chain antibody (Abcam), 1:300 for ICC; α-Tubulin, 1:10,000 for WB and acetylated-α-Tubulin antibodies, 1:10,000 for WB (both Sigma); antibodies to CNPase, 1:1,000 for WB; Non-phosphorylated neurofilaments, 1:20,000 for ICC, 1:500 for IHC on human sections; MBP, 1:1,000 for ICC; GFAP, 1:1,000 for ICC (all Sternberger Monoclonal Inc.); anti-KIF2A (Abcam), 1:20,000–40,000 for WB; anti-HDAC1 (Affinity BioReagents), 1:4,000 for ICC and WB; anti-HDAC1, 1:100 of IHC and ICC, 1:500 for WB; anti-HDAC2, 1:100 for IHC, 1:1,000 for WB; anti-HDAC3, 1:200 for ICC, 1:1,000 for WB; anti-HDAC4, 1:200 for ICC, 1:1,000 for WB; anti-HDAC5, 1:1,000 for WB; anti-HDAC6, 1:50 to 1:200 for IHC and 1:200 for WB; anti-HDAC7, 1:1,000 for WB; anti-HDAC8, 1:50 for IHC (all Santa Cruz Biotechnology); anti-HDAC3 (Abcam), 1:1,000 for IHC; anti-HDAC4 (Upstate), 1:100 for IHC; anti-HDAC5 (Cell Signaling), 1:100 for IHC; anti-HDAC7 (Cell Signaling), 1:100 for IHC; anti-FLAG (Sigma), 1:1,000 for ICC and WB; anti-CRM1 (BD Transduction Lab), 1:1,000 for WB; anti-dynamin (Abcam), 1:2,000 for WB; anti-KIF5 (Abcam), 1:2,000 for WB; anti-Tuj1 (Covance), 1:1,000 for ICC; anti-Histone H3 (Abcam), 1:2,000 for WB; anti-acetyl-Histone H3 (Upstate), 1:5,000 for WB; anti-O4 hybridoma supernatant (1:10, a gift from Dr. Bansal, University of Farmington, Farmington, CT); anti-GFP (Chemicon), 1:1,000 for ICC

In vivo model of demyelination

For details regarding the cuprizone model of demyelination, please refer to previous papers[31],[32]. Mice were maintained in sterile pathogen-free conditions under Institutional Animal Care and Use Committee of Robert Wood Johnson Medical School/UMDNJ and Mount Sinai School of Medicine. For immunohistochemistry, mice were perfused with 4% paraformaldehyde (PFA) in 0.1M phosphate buffer and the brains maintained in 30% sucrose. For RNA or protein extracts the region of the corpus callosum was dissected and frozen.

Primary cultures

Primary oligodendrocytes and astrocytes were cultured from postnatal day 1 rat pups as described previously[31]. Hippocampi and cortices were dissected from E18 rat or mouse embryos in the 1x Hanks' buffered salt solution Hanks' buffered salt solution (HBSS) (GIBCO). After digestion with 0.025% Trypsin-EDTA for 20min at 37°C, cells were incubated with NM10 medium: DMEM (GIBCO) with 10% FBS (GIBCO) for 5 min at room temperature (RT). Cells were then resuspended in neuronal culture medium: neurobasal supplemented with B27, 10mM GlutaMax (all GIBCO) and 1% penicillin-streptomycin (Sigma). After mechanical dissociation through a pipette, followed by passing

into a 22G1½ syringe gauge, cells were filtered through a cell strainer (BD Falcon) and maintained at 37°C in 5% CO_2 incubator. Three days after plating, 5nM Ara-C (Sigma) was added to the culture medium to avoid glial contamination. The following day, cells were fed with fresh neuronal medium and incubated for additional 11–12 days at 37°C, in 5% CO_2 incubator. Treatment with murine TNF-α (Chemicon), glutamate (Sigma), EDTA (Sigma), leptomycin B (Sigma), MS-275 (from Dr. Nestler, Mount Sinai School of Medicine) and tubacin (a gift of Dr. Schreiber, Broad Institute, MIT, Boston, MA) were performed at the concentrations indicated in the text. After fixing cells with 1% PFA for 20 minutes at RT, cells were post-fixed with 100% methanol for 5 minutes at −20°C.

Cerebellar slice cultures

Slice cultures were obtained by dissecting postnatal day 10 cerebella from C57BL/6J mice and cutting them into 400μm slices using a Tissue Chopper (SD Instruments). Slices were placed on collagen-coated Millicell-CM culture inserts (Millipore) and grown in medium containing 50% basal medium with Earle's salts, 25% HBSS, 25% horse serum (all GIBCO), 5mg/ml glucose and 1% penicillin-streptomycin, in 5% CO_2 incubator. Demyelination was induced after 10 days in culture, by adding 0.5mg/ml lysolecithin and 200ng/ml lipopolysaccharides (LPS) (both from Sigma), to the medium for 15–17 hours. The following day, the medium was replaced with fresh medium containing 200ng/ml LPS for an additional 24 hours. Slices were fixed with 1% PFA, post-fixed in −20°C 100% methanol and then processed for immunostaining.

Time-lapse video microscopy

For the time-lapse imaging of fluorescence labeled mitochondria, primary neurons were plated at a density of 2.5×10^5 into 35mm cover-glass bottom dishes (Willco Wells) or 3×10^4 into 8-well cover-glass bottom slides (Nunc) and maintained for 14 days in neuronal culture medium. Mitochondria were labeled with 20nM of the lipophilic mitochondrial dye MitoTracker (Invitrogen) for 30 minutes at 37°C. The medium was then replaced with fresh neuronal culture medium without PhenolRed (GIBCO) supplemented with 50μM glutamate/200ng/ml TNF-α. At each indicated time point, live cell images were captured every 5 seconds for 5 minutes using the AxioObserver.Z1 inverted fluorescence microscope equipped with controlled humidity, temperature and CO_2 incubation system (Carl Zeiss MicroImaging, Inc.). A 63× oil immersion objective was used to acquire images. Analysis of mitochondrial movement was performed using ImageJ and the AxioVision Rel.4.7 program (Carl Zeiss MicroImaging, Inc.).

To examine the relationship between morphological changes and progression of axonal damage, we used differential interference contrast (DIC) imaging and images were captured every 20–30 minutes for 12–16 hours using AxioObserver.Z1 (Zeiss).

Immunohistochemistry and Immunocytochemistry

Immunohistochemistry and immunocytochemistry were performed as described previously[31]. Immunoreactive cells were visualized using confocal microscopy (LSM510 or LSM710 Meta confocal laser scanning microscope; Carl Zeiss MicroImaging, Inc.). Fixed frozen tissue blocks from 3 controls and 4 secondary progressive multiple sclerosis (SPMS)

cases from the UK MS brain bank were processed for Luxol fast blue/periodic acid Schiff staining to identify areas of white matter demyelination. The same sections were also stained with anti-HDAC1, anti-SMI32 and anti-HDAC6 antibodies, following citrate buffer microwave retrieval, and directly bound secondary conjugates (goat anti-rabbit Alexa Fluor 488, goat anti-mouse Alexa Fluor 546). Twenty–nine areas of interest from 5 lesion containing tissue blocks from four MS cases were scrutinized for HDAC1, HDAC6 and SMI32 immunoreactivity.

Silencing experiments

For efficiency and specificity of silencing, 4×10^4 hippocampal neurons were plated in 8-well chamber slides (Nunc) and cultured for 10–11 days at 37°C, 5% CO_2 incubator. Infection with the MISSION TurboGFP shRNA Control Transduction Particles (Sigma) was conducted at MOI=20, in the presence of 4μg/ml hexamethrine bromide (Sigma) at 37 °C for 2 hours. Cultures were then maintained in medium for 72 hours at 37°C, 5% CO_2 incubator. Infection efficiency was assayed by immunocytochemistry, using antibodies against GFP and NFs. The percentage of infected cells was calculated as the number of GFP^+ cells divided by the total number of DAPI nuclei per field.

For immunocytochemistry (4×10^4 hippocampal neurons in 8-well chamber slides), quantitative PCR (3×10^5 hippocampal neurons in 6-well plates) and immunoprecipitation (2×10^6 cortical neurons in 15cm dishes), primary neurons were cultured for 10–11 days and then infected with lentiviral shRNA constructs from Sigma (MISSION shRNA). For each isoform, 4 shRNA constructs were tested and only those achieving more than 50% reduction of target are listed below. For *Hdac1* shRNA#399: CCGGGCTTGGGTAATAGCAGCCATTCT CGAGAATGGCTGCTATTACCCAAGCTTTTTG and sh#401: CCGGCCCTACAATGACTACTTTGAACTCGAG TTCAAAGTAGTCATTGTAGGGTTTTTG; For *Hdac2* shRNA#396: CCGGGCTGTGAAATTAAACCGGCAAC TCGAGTTGCCGGTTTAATTTCACAGCTTTTTG; For *Hdac3* shRNA#389: CCGGCGTGGCTCTCTGAAACCT TAACTCGAGTTAAGGTTTCAGAGAGCCACGTTTTTG; For *Hdac4* shRNA,#253: CCGGACTCTCTGATTGAG GCGCAAACTCGAGTTTGCGCCTCAATCAGAGAGTTTTTTG; For *Hdac6* shRNA, #416: CCGGCCTGGGAA AGAATCTACTCTACTCGAGTAGAGTAGATTCTTTCC; For *Hdac8* shRNA#001: CCGGGTGGATTTGGATCT ACACCATCTCGAGATGGTGTAGATCCAAATCCACTTTT TG (all from Sigma). Neurons were infected with MISSION shRNA Lentiviral Particles (MOI=20) in the presence of 4μg/ml hexamethrine bromide (Sigma). Mock controls consisted of neuronal cultures incubated with 4μg/ml hexamethrine bromide. Cells were treated with 50μM glutamate/200ng/ml TNF-α for 20 minutes or 2 hours and then processed for immunocytochemistry, quantitative PCR or immunoprecipitation.

Transfection

4×10^4 hippocampal neurons were plated in 8-well chamber slides and cultured in neuronal culture medium for 11–12 days at 37°C in 5% CO_2 incubator. The cultures were transfected with C-terminal FLAG-tagged HDAC isoforms in the pBJ5 mammalian expression vector (the gift from Dr. Schreiber, Broad Institute, MIT, Boston, MA) using the CalPhos™ Mammalian Transfection Kit (Invitrogen). 72 hours after transfection, cultures were treated with 50μM glutamate/200ng/ml TNF-α for 2 hours and then fixed for immunocytochemistry.

To examine the potential region of interaction between CRM1 and HDAC1, we generated point mutations within the nuclear export sequence identified in HDAC1 using the QuickChange II SL Site-Directed Mutagenesis Kit (Stratagene) according to the manufacturer's instruction. All leucine amino acid residues at positions 158, 161, 163 and 164 of HDAC1 in the pBJ5 vector were replaced to alanine. Wild type or mutant HDAC1 vectors were then transfected into 293T cells using FuGENE®6 (Roche), following the manufacturer's instructions. 24 hours later, protein extracts from transfected cells were processed for immunoprecipitation experiment.

MALDI-TOF Mass spectrometry

Total proteins of corpus callosum from normal and 4–week cuprizone treated mice or from untreated and treated neurons were extracted with the same method use for co-immunoprecipitation. 5–8mg of whole protein extracts were incubated with 3μg of anti-HDAC1 or HDAC6 antibody overnight at 4°C. After separation on a 12% SDS-PAGE (BioRad) proteins were stained with SilverSNAP Stain (PIERCE). Bands with a differential pattern between control and cuprizone or untreated and treated cultures, were excised and the protein sequences were analyzed by Matrix Assisted Laser Desorption/Ionization Time-of-Flight (MALDI-TOF) Mass Spectrometry (Center for Advanced Proteomics Research, Newark, NJ; Center for Advanced Biotechnology and Medicine, Piscataway, NJ).

Co-immunoprecipitation and western blot analysis

Total proteins from tissue or cultured neurons were extracted using a lysis buffer containing 50mM Hepes (pH 7.4), 150mM NaCl, 1% NP-40, 1mM dithiothreitol (DTT), 1mM ethylene diaminetetra acetic acid (EDTA), 0.01% phenylmethylsulfonyl fluoride (PMSF), 1mM aprotinin and 1mM leupeptin. Homogenized tissue or harvested primary neurons were incubated in lysis buffer for 20min on ice. After sonication on ice at the highest output (30s each, three times, cells were kept on ice for 1 min between each pulse), 1.5–2.0 mg of protein extracts were incubated overnight at 4°C with 2 μg of antibody. Immunoprecipitated samples and whole cell lysates were separated on an SDS-PAGE and transferred onto a PVDF (Millipore) membrane using a buffer containing 25mM Tris base, pH 8.3, 192mM glycine, 20% methanol for 1 hour at 100V at 4°C. Western blot analysis was performed using the appropriate dilution of primary antibodies. Immunoreactive bands were visualized using horseradish peroxidase-conjugated secondary antibodies (Amersham), followed by chemiluminescence with ECL-plus Western Blotting Detection System (Amersham).

Quantitative RT-PCR

Cells were collected in Trizol® Reagent and RNA was isolated following manufacturer's instruction and cleaned using RNeasy Mini kit (Qiagen, Hilden, Germany). 0.5–1μg of total RNA was used in 20μl of reverse transcription (RT) reaction, using SuperScript RT-PCR kit (Invitrogen, Carlsbad, CA). Quantitative RT-PCR was performed using Applied Biosystems SYBR green PCR master mix in 384-well plate in ABI 7900HT Sequence Detection PCR System. The PCR was performed in a 20μl reaction mixture containing 0.2μl cDNA as template and 100nM specific oligonucleotide primer pairs using program denaturation at 95°C for 15s; annealing and extension at 60°C for 1min for 40 cycles. Melting curve of each sample was measured to ensure the specificity of the products. Data were normalized to the internal control *GAPDH* and analyzed using Pfaffl ΔΔ Ct method.

Statistical Method

Results are expressed as mean ± standard deviation (SD) or standard error (SE) and statistically analyzed using two tailed Student's *t* tests. *P* of <0.05 was considered to be statistically significant.

Supplementary Material

Refer to Web version on PubMed Central for supplementary material.

Acknowledgments

The study was supported by NIH-RO1 NS-42925 (PCB) and NMSS RG-3957. JYK salary was supported in part also by grant n. 07-3203-BIR-E-0 from the NJ Commission on Traumatic Brain injury and CB1-0704-2 from The Christopher and Dana Reeve Foundation to PCB. We thank the UCLA Brain Bank and the UK MS Tissue Bank at Imperial College of London for providing the MS tissue samples, Dr. Christian Seiser (University of Vienna) for providing the antibodies against the N-terminal domain of the molecule, Ms. Pedre and Mr. Li for rodent handling, Dr. S Schreiber (Broad Institute at MIT) for tubacin, Dr. E Nestler and H Covington (Mount Sinai School of Medicine) for MS-275, Ms. S. Lagger (University of Vienna) for sharing unpublished results and critical comments on the manuscript, Dr. P. Lobel (Rutgers University) for discussions regarding MALDI-TOF data, Drs. J. Zheng (Emory University) and Dr. K. Teng (Weil Medical College) for helpful discussion and Mr. Ralph Rosa for the support of the NJ Multiple Sclerosis Research Foundation.

References

1. Galvin JE, Uryu K, Lee VM, Trojanowski JQ. Axon pathology in Parkinson's disease and Lewy body dementia hippocampus contains alpha-, beta-, and gamma-synuclein. Proc Natl Acad Sci U S A. 1999; 96:13450–5. [PubMed: 10557341]
2. Ferguson B, Matyszak MK, Esiri MM, Perry VH. Axonal damage in acute multiple sclerosis lesions. Brain. 1997; 120 (Pt 3):393–9. [PubMed: 9126051]
3. Trapp BD, et al. Axonal transection in the lesions of multiple sclerosis. N Engl J Med. 1998; 338:278–85. [PubMed: 9445407]
4. Dutta R, Trapp BD. Pathogenesis of axonal and neuronal damage in multiple sclerosis. Neurology. 2007; 68:S22–31. discussion S43–54. [PubMed: 17548565]
5. Trapp BD, Stys PK. Virtual hypoxia and chronic necrosis of demyelinated axons in multiple sclerosis. Lancet Neurol. 2009; 8:280–91. [PubMed: 19233038]
6. Beirowski B, et al. The progressive nature of Wallerian degeneration in wild-type and slow Wallerian degeneration (WldS) nerves. BMC Neurosci. 2005; 6:6. [PubMed: 15686598]
7. Fisher E, et al. Imaging correlates of axonal swelling in chronic multiple sclerosis brains. Ann Neurol. 2007; 62:219–28. [PubMed: 17427920]

8. Stokin GB, et al. Axonopathy and transport deficits early in the pathogenesis of Alzheimer's disease. Science. 2005; 307:1282–8. [PubMed: 15731448]
9. Watson DF, Fittro KP, Hoffman PN, Griffin JW. Phosphorylation-related immunoreactivity and the rate of transport of neurofilaments in chronic 2,5-hexanedione intoxication. Brain Res. 1991; 539:103–9. [PubMed: 1707736]
10. Yabe JT, Pimenta A, Shea TB. Kinesin-mediated transport of neurofilament protein oligomers in growing axons. J Cell Sci. 1999; 112 (Pt 21):3799–814. [PubMed: 10523515]
11. Pant HC. Dephosphorylation of neurofilament proteins enhances their susceptibility to degradation by calpain. Biochem J. 1988; 256:665–8. [PubMed: 2851997]
12. Perez-Olle R, et al. Mutations in the neurofilament light gene linked to Charcot-Marie-Tooth disease cause defects in transport. J Neurochem. 2005; 93:861–74. [PubMed: 15857389]
13. Kiaei M, et al. Celastrol blocks neuronal cell death and extends life in transgenic mouse model of amyotrophic lateral sclerosis. Neurodegener Dis. 2005; 2:246–54. [PubMed: 16909005]
14. Song SK, et al. Demyelination increases radial diffusivity in corpus callosum of mouse brain. Neuroimage. 2005; 26:132–40. [PubMed: 15862213]
15. Wegner C, Esiri MM, Chance SA, Palace J, Matthews PM. Neocortical neuronal, synaptic, and glial loss in multiple sclerosis. Neurology. 2006; 67:960–7. [PubMed: 17000961]
16. Stone JR, et al. Impaired axonal transport and altered axolemmal permeability occur in distinct populations of damaged axons following traumatic brain injury. Exp Neurol. 2004; 190:59–69. [PubMed: 15473980]
17. Bitsch A, Schuchardt J, Bunkowski S, Kuhlmann T, Bruck W. Acute axonal injury in multiple sclerosis. Correlation with demyelination and inflammation. Brain. 2000; 123 (Pt 6):1174–83. [PubMed: 10825356]
18. King AE, et al. Excitotoxicity mediated by non-NMDA receptors causes distal axonopathy in long-term cultured spinal motor neurons. Eur J Neurosci. 2007; 26:2151–9. [PubMed: 17908171]
19. Williamson TL, Cleveland DW. Slowing of axonal transport is a very early event in the toxicity of ALS-linked SOD1 mutants to motor neurons. Nat Neurosci. 1999; 2:50–6. [PubMed: 10195180]
20. Adams JH, Graham DI, Gennarelli TA, Maxwell WL. Diffuse axonal injury in non-missile head injury. J NeurolNeurosurg Psychiatry. 1991; 54:481–3.
21. de Ruijter AJ, van Gennip AH, Caron HN, Kemp S, van Kuilenburg AB. Histone deacetylases (HDACs): characterization of the classical HDAC family. Biochem J. 2003; 370:737–49. [PubMed: 12429021]
22. Yang XJ, Gregoire S. Class II histone deacetylases: from sequence to function, regulation, and clinical implication. Mol Cell Biol. 2005; 25:2873–84. [PubMed: 15798178]
23. Yao YL, Yang WM, Seto E. Regulation of transcription factor YY1 by acetylation and deacetylation. Mol Cell Biol. 2001; 21:5979–91. [PubMed: 11486036]
24. Chen Z, et al. Induction and superinduction of growth arrest and DNA damage gene 45 (GADD45) alpha and beta messenger RNAs by histone deacetylase inhibitors trichostatin A (TSA) and butyrate in SW620 human colon carcinoma cells. Cancer Lett. 2002; 188:127–40. [PubMed: 12406558]
25. Hubbert C, et al. HDAC6 is a microtubule-associated deacetylase. Nature. 2002; 417:455–8. [PubMed: 12024216]
26. Chawla S, Vanhoutte P, Arnold FJ, Huang CL, Bading H. Neuronal activity-dependent nucleocytoplasmic shuttling of HDAC4 and HDAC5. J Neurochem. 2003; 85:151–9. [PubMed: 12641737]
27. Kawaguchi Y, et al. The deacetylase HDAC6 regulates aggresome formation and cell viability in response to misfolded protein stress. Cell. 2003; 115:727–38. [PubMed: 14675537]
28. Dompierre JP, et al. Histone deacetylase 6 inhibition compensates for the transport deficit in Huntington's disease by increasing tubulin acetylation. J Neurosci. 2007; 27:3571–83. [PubMed: 17392473]
29. Schumacher PA, Eubanks JH, Fehlings MG. Increased calpain I-mediated proteolysis, and preferential loss of dephosphorylated NF200, following traumatic spinal cord injury. Neuroscience. 1999; 91:733–44. [PubMed: 10366029]

30. Pitt D, Werner P, Raine CS. Glutamate excitotoxicity in a model of multiple sclerosis. Nat Med. 2000; 6:67–70. [PubMed: 10613826]
31. Shen S, et al. Age-dependent epigenetic control of differentiation inhibitors is critical for remyelination efficiency. Nat Neurosci. 2008; 11:1024–34. [PubMed: 19160500]
32. Li J, et al. Inhibition of p53 transcriptional activity: a potential target for future development of therapeutic strategies for primary demyelination. J Neurosci. 2008; 28:6118–27. [PubMed: 18550754]
33. Birgbauer E, Rao TS, Webb M. Lysolecithin induces demyelination in vitro in a cerebellar slice culture system. J Neurosci Res. 2004; 78:157–66. [PubMed: 15378614]
34. Bruck W. The pathology of multiplesclerosis is the result of focal inflammatory demyelination with axonal damage. J Neurol. 2005; 252 (Suppl 5):v3–9. [PubMed: 16254699]
35. Ouardouz M, et al. Glutamate receptors on myelinated spinal cord axons: II. AMPA and GluR5 receptors. Ann Neurol. 2009; 65:160–6. [PubMed: 19224531]
36. Kurnellas MP, Donahue KC, Elkabes S. Mechanisms of neuronal damage in multiple sclerosis and its animal models: role of calcium pumps and exchangers. Biochem Soc Trans. 2007; 35:923–6. [PubMed: 17956247]
37. Wen W, Meinkoth JL, Tsien RY, Taylor SS. Identification of a signal for rapid export of proteins from the nucleus. Cell. 1995; 82:463–73. [PubMed: 7634336]
38. Wolff B, Sanglier JJ, Wang Y. Leptomycin B is an inhibitor of nuclear export: inhibition of nucleo-cytoplasmic translocation of the human immunodeficiency virus type 1 (HIV-1) Rev protein and Rev-dependent mRNA. Chem Biol. 1997; 4:139–47. [PubMed: 9190288]
39. Uo T, Veenstra TD, Morrison RS. Histone deacetylase inhibitors prevent p53-dependent and p53-independent Bax-mediated neuronal apoptosis through two distinctmechanisms. J Neurosci. 2009; 29:2824–32. [PubMed: 19261878]
40. Dasmahapatra G, Almenara JA, Grant S. Flavopiridol and histone deacetylase inhibitors promote mitochondrial injury and cell death in human leukemia cells that overexpress Bcl-2. Mol Pharmacol. 2006; 69:288–98. [PubMed: 16219908]
41. Morrison BE, et al. Neuroprotection by histone deacetylase-related protein. Mol Cell Biol. 2006; 26:3550–64. [PubMed: 16611996]
42. Ballas N, et al. Regulation of neuronal traits by a novel transcriptional complex. Neuron. 2001; 31:353–65. [PubMed: 11516394]
43. Zhang Y, et al. HDAC-6 interacts with and deacetylates tubulin and microtubules in vivo. Embo J. 2003; 22:1168–79. [PubMed: 12606581]
44. Bolger TA, Yao TP. Intracellular trafficking of histone deacetylase 4 regulates neuronal cell death. J Neurosci. 2005; 25:9544–53. [PubMed: 16221865]
45. Hoshino M, et al. Histone deacetylase activity is retained in primary neurons expressing mutant huntingtin protein. J Neurochem. 2003; 87:257–67. [PubMed: 12969272]
46. Morfini GA, et al. Axonal transport defects in neurodegenerative diseases. J Neurosci. 2009; 29:12776–86. [PubMed: 19828789]
47. Gu H, Liang Y, Mandel G, Roizman B. Components of the REST/CoREST/histone deacetylase repressor complex are disrupted, modified, and translocated in HSV-1-infected cells. Proc Natl Acad Sci U S A. 2005; 102:7571–6. [PubMed: 15897453]
48. Zhang Y, Jones C. The bovine herpesvirus 1 immediate-early protein (bICP0) associates with histone deacetylase 1 to activate transcription. J Virol. 2001; 75:9571–8. [PubMed: 11559788]
49. Viatour P, et al. Cytoplasmic IkappaBalpha increases NF-kappaB-independent transcription through binding to histone deacetylase (HDAC) 1 and HDAC3. J Biol Chem. 2003; 278:46541–8. [PubMed: 12972430]

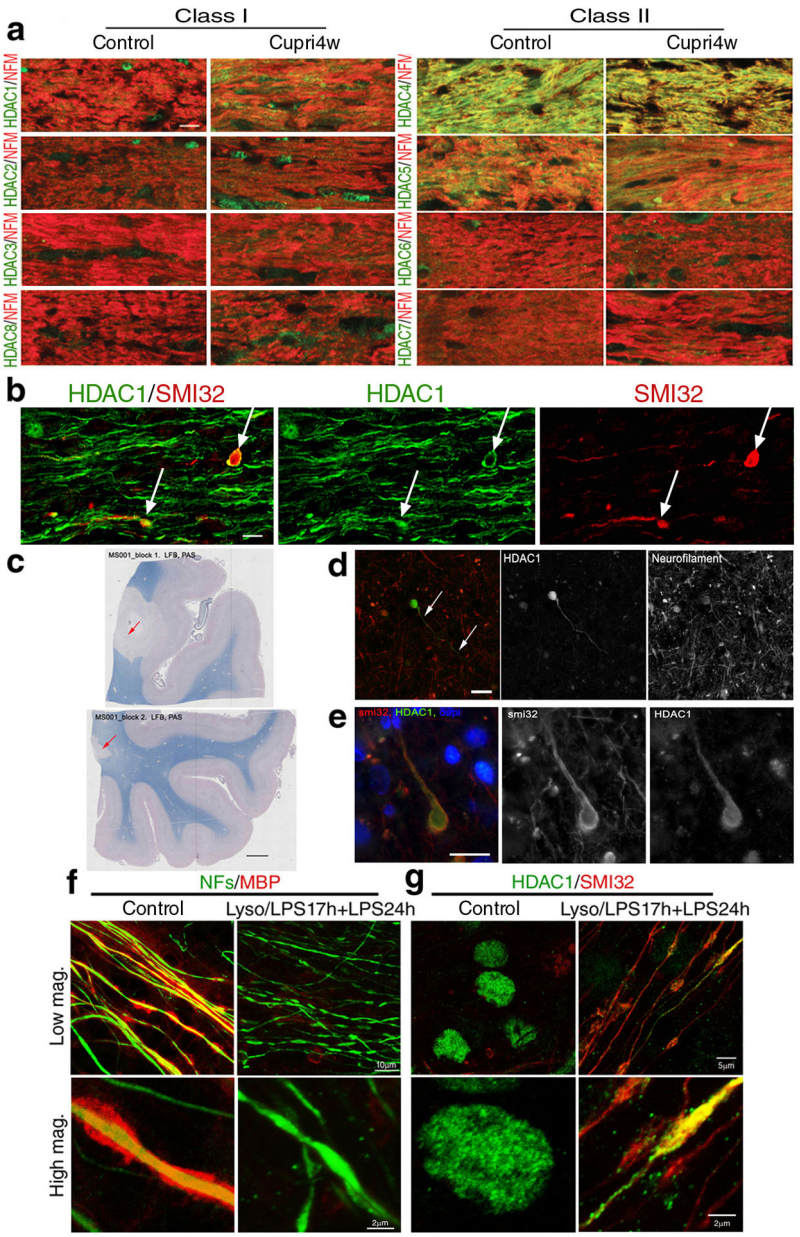

Figure 1. Cytosolic HDAC1 is detected in animal models of demyelination, in the brain of MS patients and in demyelinated slice cultures

(a) Confocal micrographs of the corpus callosum of control and 4 week cuprizone-fed mice (Cupri4w), stained with antibodies specific for class I (HDAC1, HDAC2, HDAC3, HDAC8) and class II HDAC isoforms (HDAC4, HDAC5, HDAC6 and HDAC7), indicated on the left (green) and with anti-neurofilament medium chain antibody (NFs, red). Scale bar 10 μm; 63× objective. (b) Confocal image of the co-localization (white arrows) of hypophosphorylated neurofilament heavy chain (SMI32, red) and HDAC1 (green) in damaged axons in the corpus callosum of cuprizone fed mice. Scale bar 5 μm. (c) Luxol fast blue/periodic acid Schiff staining of human brain sections identified areas of white matter demyelination (arrows, scale bar 200 μm). (d) Serial sections of the same lesions were used

to show the presence of HDAC1^{+} end bulbs (green) in neurofilament positive (red) axons. Scale bar 10 μm. (e) Adjacent sections were processed for immunohistochemistry with antibodies for SMI32 (red) and HDAC1 (green) in white matter lesions. DAPI (blue) was used as nuclear counterstain. Scale bar 10 μm. (f) Confocal images of cerebellar slice cultures either untreated (Control) or treated with lysolecithin and LPS to induce demyelination (Lyso/LPS17h+LPS24h). Cultures were stained with antibodies specific for myelin basic protein (MBP, red) and NFs (green) antibodies. (g) The same cultures were then stained for HDAC1 (green) and SMI32 (red).

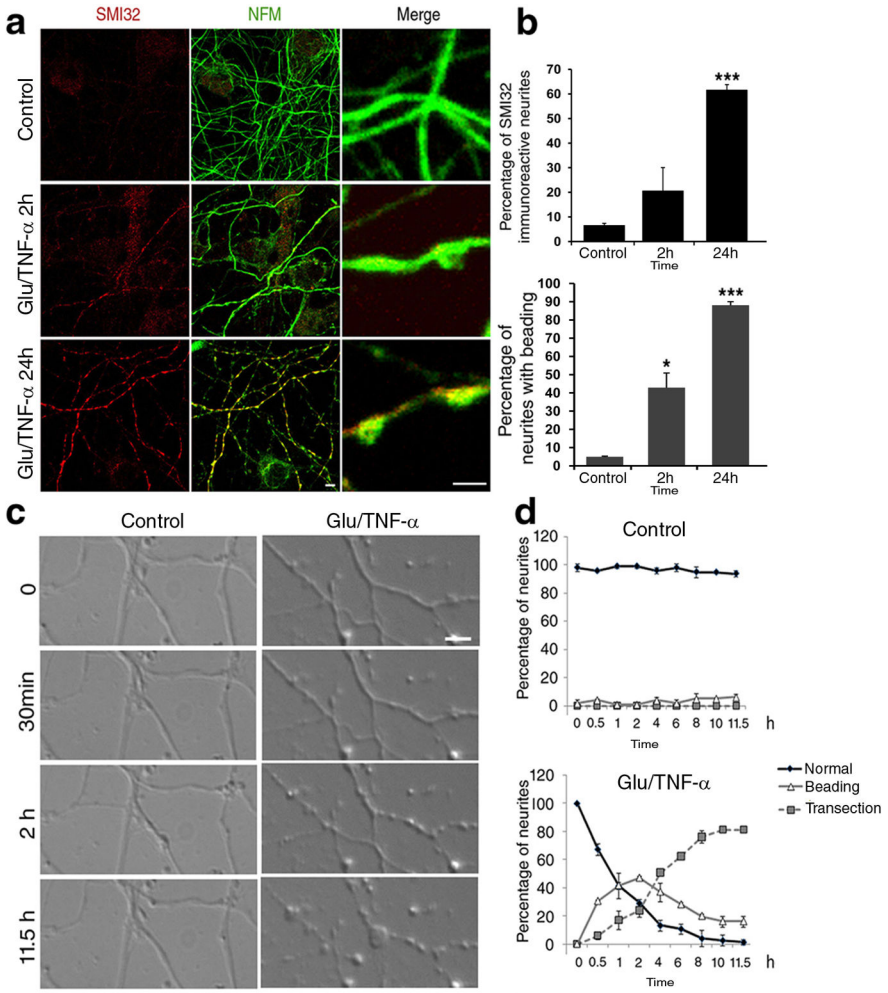

Figure 2. Glutamate and TNF-α treatment of primary neuronal cultures induces neuritic beading followed by transections

(a) Confocal image of cultured neurons either untreated (Control) or treated with 50μM glutamate/200ng/ml TNF-α for 2 or 24 hours. Cells were stained with antibodies for NFM (green) to visualize neurites and SMI32 (red) to identify damaged neurites. Scale bar 10μm in low and 2 μm in high magnification. (b) Bar graphs show the percentage of $SMI32^+$ beaded neurites relative to the total number of NFM^+ neurites (mean ± SD, $n = 83\pm12$ neurites counted in each condition. * $P < 0.05$, *** $P < 0.001$ two-tailed Student's t-test). (c) Time-lapse video microscopy of cultured neurons exposed to 50μM glutamate/200ng/ml TNF-α. Images were captured every 30 minutes for 12 hours. Scale bar 5μm. (d) The graph indicates the percentage of normal appearing, beaded and transected neurites, relative to the total, at each time point. Error bars represent standard deviation.

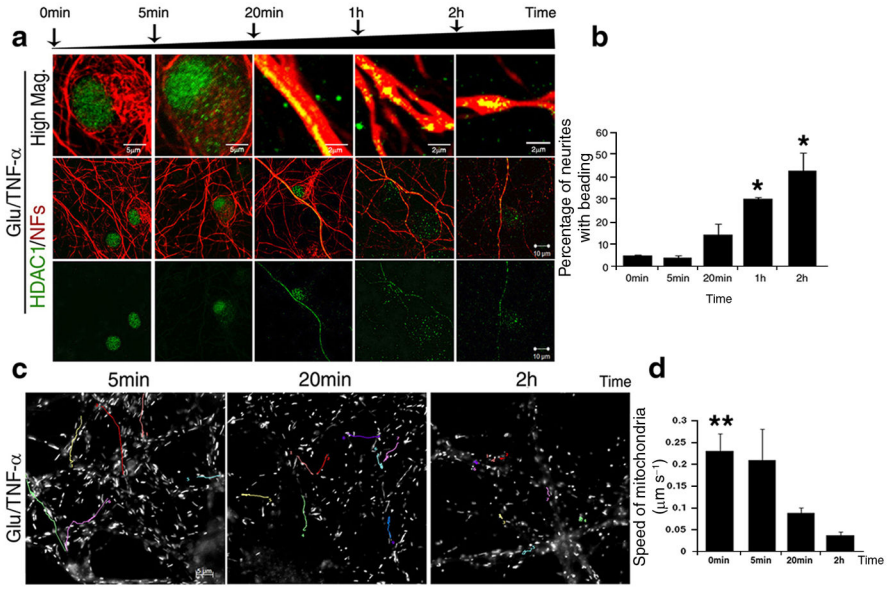

Figure 3. Cytosolic localization of HDAC1 precedes the onset of localized beadings and impaired mitochondrial transport

(a) Confocal images of neurons before and after exposure to 50μM glutamate/200ng/ml TNF-α for the indicated time periods. Control and treated cultures were co-stained with antibodies specific for HDAC1 (green) and for neurofilament medium and light chains (NFs, red). Upper panel, scale bar 5μm or 2 μm; lower panels 10 μm. (b) Bar graphs indicate the percentage of beaded neurites relative to the total NFs^+ population at the indicated time points; error bars represent standard deviation. $*P < 0.05$. (c) Live cell images of moving mitochondria, labelled with MitoTracker in neurons exposed to 50μM glutamate/200ng/ml TNF-α. The position of each mitochondrion was recorded every 5 seconds for 5 minutes at the indicated time points and the tracks of mitochondrial movement were pseudocolored. Scale bar 5μm. (d) Bar graphs indicate the average speed of moving mitochondria with standard deviation. $**P < 0.01$.

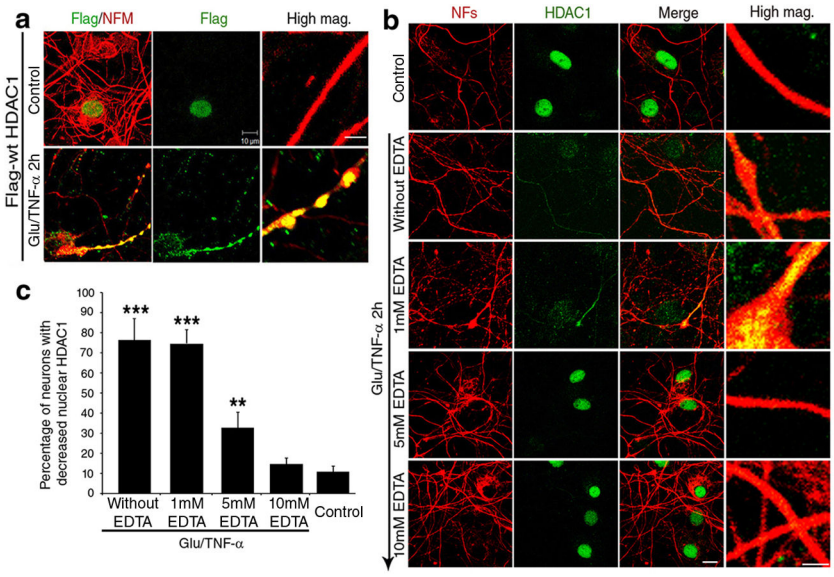

Figure 4. Calcium-depletion prevents HDAC1 nuclear export and the onset of neuritic beading induced by glutamate and TNF-α treatment

(a) Confocal image of primary cultures transfected with FLAG-tag-HDAC1 on day 10 and then analyzed three days later in the absence (Control) or presence of 50μM glutamate/ 200ng/ml TNF-α for 2 hours. Transfected cells were detected using antibodies against FLAG-tag (green) and NFM (red). Scale bar 2 μm for high magnification and 10 μm for low magnification. (b) Confocal images of cultured neurons pre-treated with increasing concentrations of the calcium chelator EDTA and stained with antibodies specific for HDAC1 (green) and NFs (red). Note that EDTA prevents neurite beading induced by treatment with 50μM glutamate/200ng/ml TNF-α. Scale bar 10μm for low magnification and 2 μm for high magnification (High mag.). (c) Bar graphs show the quantification of the results shown in (b) (mean ± SD; $^{**}P < 0.01$, $^{***}P < 0.001$).

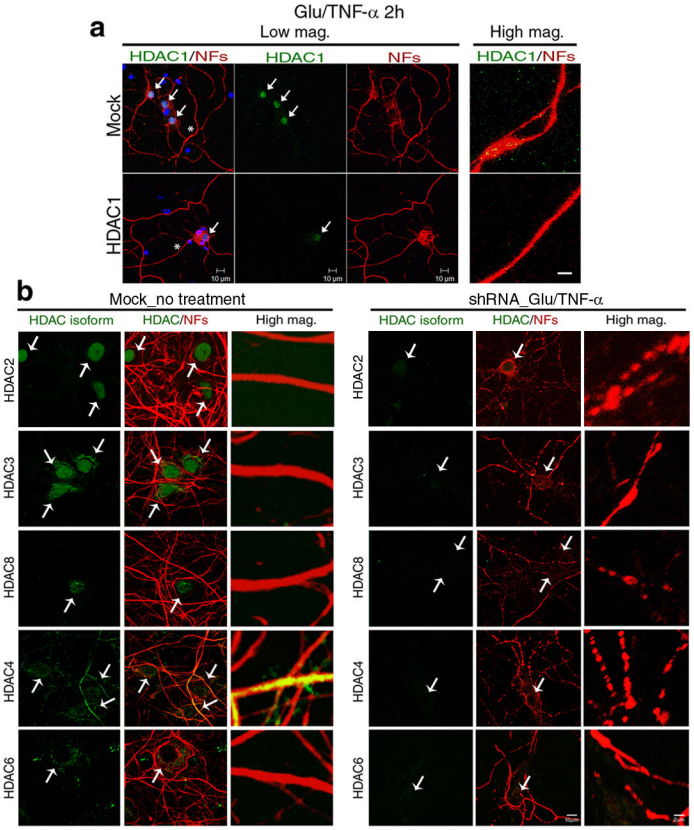

Figure 5. Silencing HDAC1, but not other isoforms prevents neurite beading

(a) Primary neurons were infected with *Hdac1*-shRNA lentiviral particles and then exposed to 50μM glutamate/200ng/ml TNF-α for 2 hours and processed for immunocytochemistry with anti-HDAC1 (green) and NFs (red) antibodies. DAPI (blue) was used as nuclear counterstain. Scale bar 10μm for low magnification and 2 μm for high magnification (High mag.). (b) Cultured neurons were infected with class I (*Hdac2*, *Hdac3* and *Hdac8*) and class II (*Hdac4* and *Hdac6*) *Hdac*-shRNA lentiviral particles. 72 hours after infection, cultures were exposed to 50μM glutamate/200ng/ml TNF-α for 2 hours and then processed for immunocytochemistry with antibodies specific for HDAC2, HDAC3, HDAC4, HDAC6, or HDAC8 (green) and NFs (red). Scale bar 10 μm for low and 2 μm for high magnification.

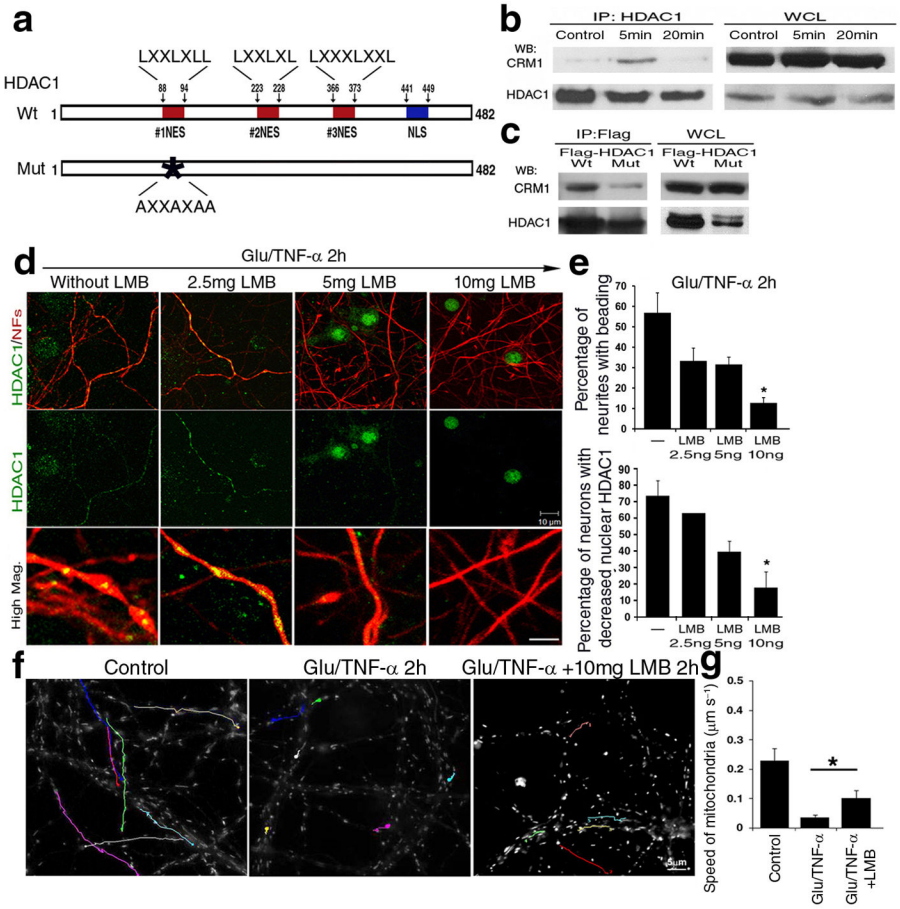

Figure 6. CRM1 dependent nuclear export of HDAC1 is essential for the induction of damage induced by glutamate and TNF-α

(a) Schematic diagram of HDAC1 protein sequence, with potential nuclear export sequences (NESs, red), and nuclear localization domains (NLS, blue). (b) Protein extracts from cultured neurons either untreated or treated with toxic stimuli for 5 or 20 minutes were immunoprecipitated with antibodies specific for HDAC1 (IP:HDAC1) and processed for western blot analysis using CRM1 or HDAC1 antibodies. Whole cell lysates (WCL) were used as controls. (c) Wild type (Wt) and NES mutant HDAC1 (Mut) over-expression, followed by immunoprecipitation with anti-FLAG antibody and western blot analysis with anti-CRM1 and FLAG antibodies. (d) Immunocytochemistry of primary neurons pre-treated with increasing concentrations of leptomycin B (LMB) for 30min, then exposed to 50μM glutamate/200ng/ml TNF-α (Gluta/TNF-α) and stained with antibodies for HDAC1 (green) and NFs (red). Scale bar 10μm for low and 2 μm for high magnification. (e) Bar graphs indicate the percentage of beaded neurites relative to the total population (mean ± SD; *$P <$ 0.05). (f) Pseudo-colored image of mitochondrial movement, using time-lapse video microscopy of primary neurons treated with LMB and exposed to glutamate and TNF-α. Untreated cultures were used as controls. Cultures were labeled with Mitotracker GreenFM and photograms were taken every 5 seconds within a 5 minute time period. Note that LMB treatment ameliorated mitochondrial movement. Scale bar 5μm. (g) Bar graphs indicate the

average speed of moving mitochondria in each condition and error bars represent standard deviation *$P < 0.05$.

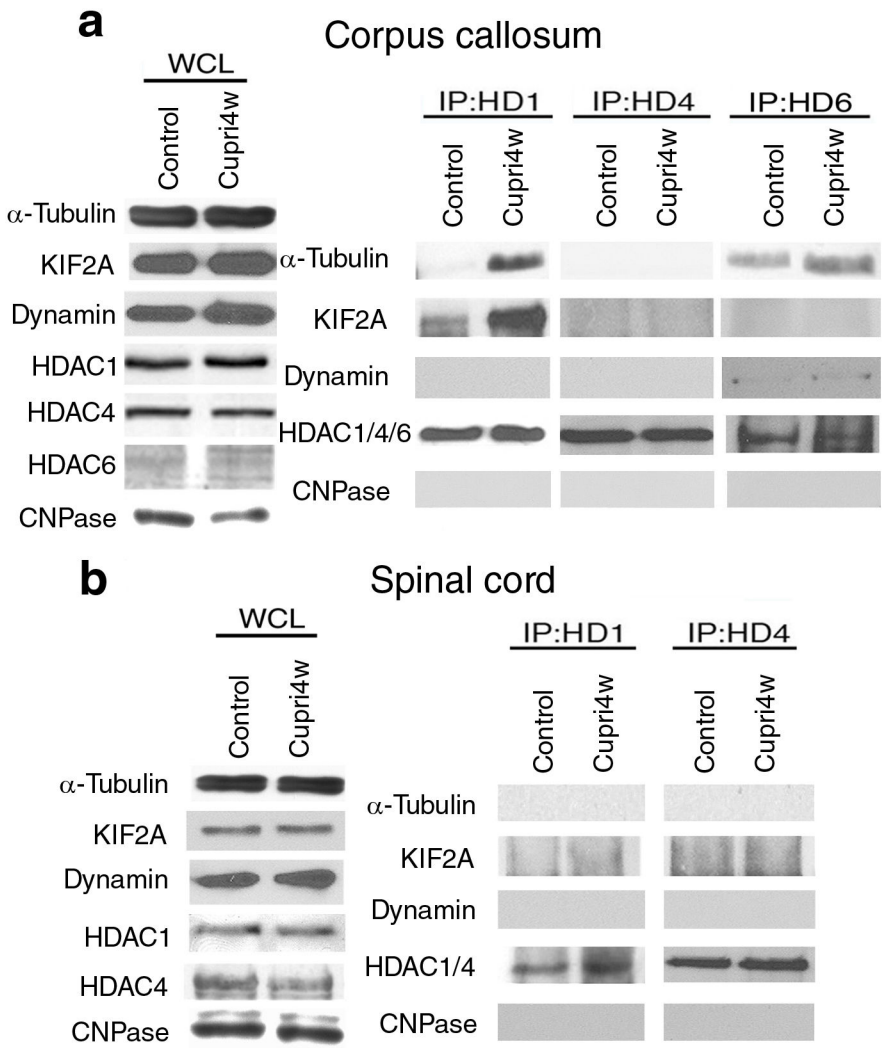

Figure 7. HDAC1 binding partners in demyelinating region of cuprizone-treated mice

(a) Validation of the MALDI-TOF results *in vivo*. Total proteins from demyelinated (Corpus callosum) and (b) non-demyelinated (Spinal cord) regions of cuprizone-treated (Cupri4w) or control mice were immunoprecipitated with anti-HDAC1, HDAC4, or HDAC6 antibody and probed with the indicated antibodies. Shown are representative results of 3 independent experiments, each comparing 3 mice for each condition. Note that HDAC1 forms protein complexes with proteins involved in axonal transport only in demyelinated regions. The expression levels of CNPase, an enzyme critical for myelination process, was used to verify the occurrence of demyelination, while expression levels of HDAC1, HDAC4 and HDAC6 were used to confirm the efficiency of the immunoprecipitation.

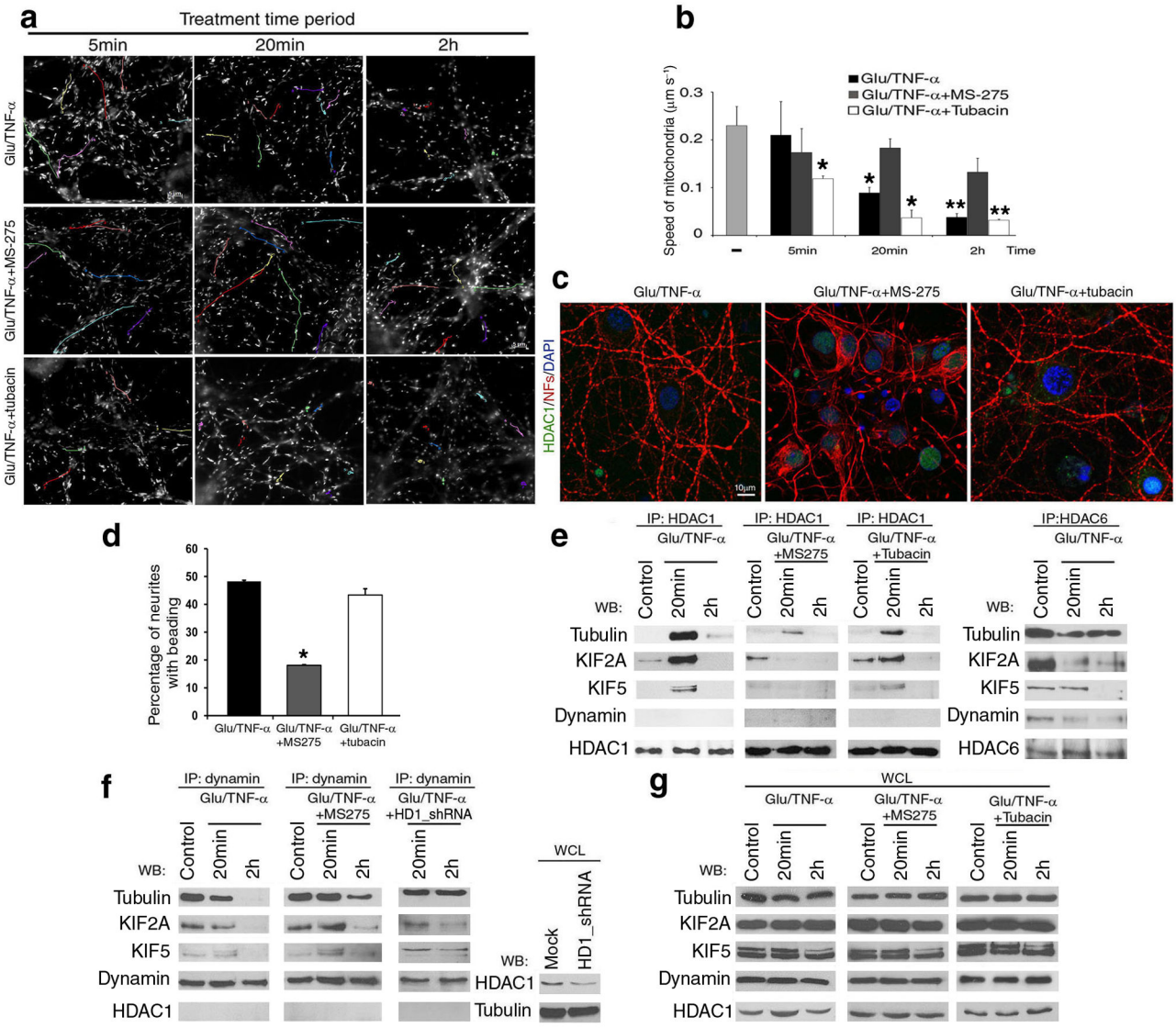

Figure 8. Activity-dependent interaction of HDAC1 with motor proteins impairs mitochondrial transport

(a) Pseudo-colored image of time-lapse video-microscopy of neuronal cultures treated with 50μM glutamate/200ng/ml TNF-α in the presence of HDAC1 inhibitor MS-275, or HDAC6 inhibitor tubacin. Mitochondrial movement was examined using the lipophilic mitochondrial dye MitoTracker. Scale bar 5μm. (b) Bar graphs indicate the average speed of moving mitochondria (mean ± SD). **P* < 0.05, ***P* < 0.01 (c) Confocal image of neurites in cultures treated with 50μM glutamate/200ng/ml TNF-α for 2 hours (Glu/TNF-α), or in the presence of MS-275 (Glu/TNF-α+MS-275) or tubacin (Glu/TNF-α+tubacin). Immunoreactivity for HDAC1 (green) and NFs (red); DAPI (blue) as nuclear counterstain. (d) Bar graphs represent the percentage of beaded neurites in (c) (Mean ± SD; **P* < 0.05). (e) Protein complexes containing HDAC1 (left) or HDAC6 (right) and motor proteins were identified by immunoprecipitation and western blot analysis. Proteins were extracted from cultured neurons treated as indicated in (a). (f) Co-immunoprecipitation with anti-dynamin antibody

of protein extracts from either untreated or MS-275 pre-treated neurons exposed to 50μM glutamate/200ng/ml TNF-α for 20min or 2 hours. Note that the association of dynamin from motors was partially restored by treatment with MS-275 or silencing HDAC1 with shRNAs. Silencing efficiency was confirmed by western blot analysis using HDAC1 antibody. (g) Western blot analysis of whole cell lysates (WCL) from cultures treated as described in (e) and (f).

Primers used in quantitative PCR.

Gene	Product size (bp)	Forward	Reverse
Bax	174	5′-CTGCAGAGGATGATTGCTGA -3′	5′-GATCAGCTCGGGCACTTTAG-3′
Bcl2	97	5′-AAGCTGTCACAGAGGGGCTA -3′	5′-CAGGCTGGAAGGAGAAGATG-3′
c-Jun	77	5′-AAAACCTTGAAAGCGCAAAA-3′	5′-TGTTTAAGCTGTGCCACCTG -3′
GAPDH	201	5′-AGACAGCCGCATCTTCTTGT -3′	5′-CTTGCCGTGGGTAGAGTCAT-3′
Hdac1	76	5′-GTGGCCCTGGACACAGAGAT -3′	5′-GCTTGAAATCCGGTCCAAAGT -3′
Hdac2	88	5′-TGAAATTAAACCGGCAACAAACT -3′	5′-CAGAACCCTGATGCTTCTGACTT-3′
Hdac3	70	5′-ATGCCTTCAACGTGGGTGAT -3′	5′-CCTGTGTAACGGGAGCAGAAC -3′
Hdac4	107	5′-AAATGAGTTTGCCCCAGATG -3′	5′-ACCCAAAACATTTGGCAGAG -3′
Hdac5	118	5′-TGACAGCCTTCAGGACAGTG -3′	5′-GAATAGCCACCCAGTGGAGA -3′
Hdac6	114	5′-TCCTCAGCTGTGTTGACCTG -3′	5′-TGTCCTCCCCAAACTTGTTC -3′
Hdac7	138	5′-ATGACGACGGCAACTTCTTC -3′	5′-AAGCAGCCAGGTACTCAGGA -3′
Hdac8	71	5′-CCCTGCATAAACAAATGAGGATAGT-3′	5′-AGTGTGGAAGGTGGCCATCTC -3′
Nav1.2	170	5′-GGTACCTCCAGGACCTGACA -3′	5′-GAAGGGATTTTCCTGCTTCC -3′
Nav1.6	158	5′-CACCATCCTGACCAACTGTG -3′	5′-GGTCTCGCAAGAAGGTGAAG-3′